Spiro[(dihydropyrazin-2,5-dione)-6,3′-(2′,3′-dihydrothieno[2,3-*b*]naphtho-4′,9′-dione)]-Based Cytotoxic Agents: Structure–Activity Relationship Studies on the Substituent at N4-Position of the Diketopiperazine Domain

Isabel Gomez-Monterrey,[†] Pietro Campiglia,[‡] Alfonso Carotenuto,[†] Paola Stiuso,[§] Alessia Bertamino,[‡] Marina Sala,[†] Claudio Aquino,[†] Paolo Grieco,[†] Silvana Morello,[‡] Aldo Pinto,[‡] Pio Ianelli,[‡] and Ettore Novellino*[,†]

Dipartimento di Chimica Farmaceutica e Tossicologica, University of Naples "Federico II", 80131 Napoli, Dipartimento di Scienze Farmaceutica, Università di Salerno, I-84084, Fisciano, Salerno, and Dipartimento di Biochimica e Biofisica "Francesco Cetrangolo", Seconda Università di Napoli, 80138 Napoli

Received October 17, 2007

Analogues of the previously reported potent cytotoxic spiro[(dihydropyrazine-2,5-dione)-6,3′-(2′,3′-dihydrothieno[2,3-*b*]naphtho-4′,9′-dione)] derivatives (**3**, **3′**) were prepared to explore new structural requirements at the diketopiperazine domain for the cytotoxic activity. The in vitro activity was evaluated against the MCF-7 human breast carcinoma and SW 620 human colon carcinoma cell lines. The 4-[(2-*N*,*N*-dimethyl)amino]ethyl (**6i**), and the 4-(2-pyrrolydin)ethyl (**6l**) derivatives emerged as the most potent compounds of this series, with a cytotoxic activity comparable to that of doxorubicin. These compounds, in both racemic and pure enantiomeric forms, showed also a high efficacy in cell lines resistant to doxorubicin (MCF-7/Dx) and in cell lines that were highly resistant to treatment with doxorubicin, such as HEK-293 (kidney), M-14 (melanoma), and HeLa (cervical adenocarcinoma) human cell lines. In addition, the effects on growth and cell cycle progression in CaCo-2 cell line (colon adenocarcinoma) and DNA-binding properties were investigated.

Introduction

Exhaustive research[1–6] has been devoted to the development of new potential anticancer agents related to anthracyclines (daunorubicin and doxorubicin) and anthracenediones (mitoxantrone), with the goal of bypassing significant problems that limit the utility of these compounds, such as the emergence of drug resistance mediated by overexpression of transporter P-glycoprotein[7,8] and severe short- and long-term side effects, in this case, mostly associated with bone marrow and myocardial cell toxicity.[9,10] In this regard and in connection with an ongoing research program aimed at discovering new quinone-based derivatives as potential cytotoxic agents, we have developed three different series of compounds containing a new planar ring system, the 3-amino-3-(ethoxycarbonyl)-2,3-dihydrothieno[2,3-*b*]naphtho-4,9-dione system (**1**, DTNQ).[11] The modifications effected on DTNQ system involved the incorporation of amino acid and dipeptide at 3-amino position (series I),[12] several alkyl-, hydroxyalkyl-, and aminoalkyl-substituted side chains through a hydantoin ring (series II),[13] and amino acid side chains inserted at position C-3 and C-3 N-4 (**3′**) of a diketopiperazine ring (series III; Figure 1).[14] During the exploration of the structure–activity relationship (SAR) in these series, we have found that the incorporation of a five- or six-membered heterocyclic to DTNQ chromophore is an effective approach to design new compounds with potent cytotoxic activity and able to overcome multidrug resistance of tumor cells. Thus, the spirohydantoin derivatives 3-[2-(*N*,*N*-dimethylamino)ethyl or propyl]-spiro[(dihydroimidazo-2,4-dione)-5,3′-(2′,3′-dihydrothieno [2,3-*b*]naphtho-4′,9′-dione)] (**2a**, **2b**), and the spirodiketopiperazine derivative spiro[(hexahydropyrrolo[1,2-*a*]pyrazine-1,4-dione)-6,3′-(2′,3′-dihydrothieno[2,3-*b*]naphtho-4′,9′-dione)] (**3′**) showed remarkable biological activity, not only against several human solid tumor cell lines (comparable to that of doxorubicin), but also toward doxorubicin- and *cis*-platinum-resistant human cell lines.[13,14] However, even though these derivatives had many of the structural characteristics similar to those of classical quinonic-based DNA intercalators, they were not able to inhibit topoisomerase II at equicytotoxic concentrations. These findings seem to indicate that other factors such as differences in cellular uptake, distribution within the cell, and an additional target within the cell might also affect the cytotoxicity of these derivatives.[15]

Taking into consideration all these data, now we have developed a novel series of 4-substituted spiro-[(dihydropyrazine-2,5-dione)-6,3′-(2′,3′-dihydrothieno[2,3-*b*]-naphtho-4′,9′-dione)] derivatives (series IV). The new series features the spirodiketopiperazine moiety of the series III with the substituents placed at position N-4. We chose, as N-4 substituents, some of the most active found in the hydantoine series (II): methyl, hydroxylethyl, hydroxylpropyl, aminoethyl, aminopropyl, (*N*,*N*-dimethyl) aminoethyl, (*N*,*N*-dimethyl)aminopropyl, and (*N*,*N*-diethyl)aminoethyl. A few groups of substituents with different chemical functionalities, thioethyl, thiopropyl, 3-imidazopropyl, 2-imidazoethyl, 2-pyrrolidinethyl, 2-piperidinethyl, and 2-morpholinethyl, were also employed. The objectives of this investigation were to define which new structural parameters are important for the cytotoxic activity, obtaining therefore higher SAR information on the DTNQ derivatives, and to explore some of the basic biochemical events correlated to their cytotoxic activity. The present paper deals with the synthesis, the cytotoxic activity, the interaction with DNA, and the mechanism of cell cycle perturbation of this new series of derivatives.

Results and Discussion

Chemistry. Initially, the synthesis of nonsubstituted spirodiketopiperazine derivative (**3**) was carried out by condensation of

* To whom correspondence should be addressed. Phone: +39-081-678643. Fax: +39-081-678644. E-mail: novellin@unina.it.
[†] University of Naples "Federico II".
[‡] Università di Salerno.
[§] Seconda Università di Napoli.

10.1021/jm7013056 CCC: $40.75
Published on Web 04/23/2008

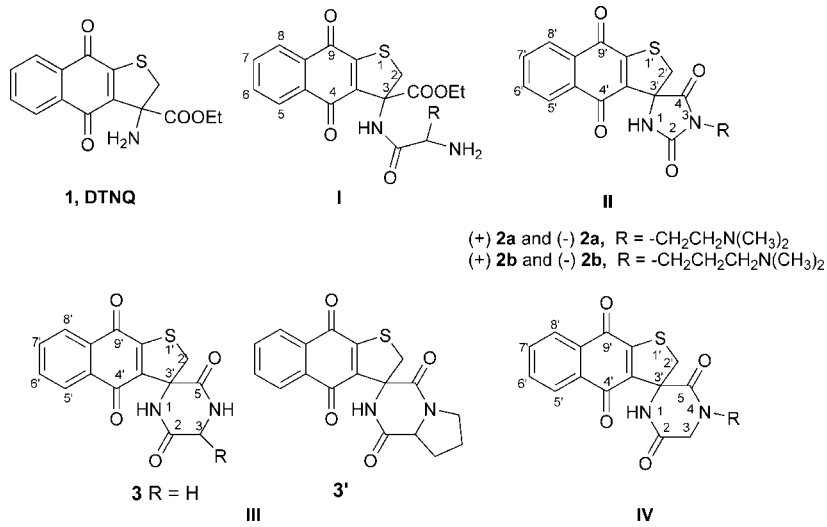

Figure 1. Structure of DTNQ template and its derivatives.

Scheme 1. Synthesis of 4-Alkyl(alkylsubstituted)spiro[(dihydropirazin-2,5-dione)-6,3′-(2′,3′-dihydrothieno[2,3-*b*]naphtho-4′,9′-dione)] Derivatives (**6a**–**p**)

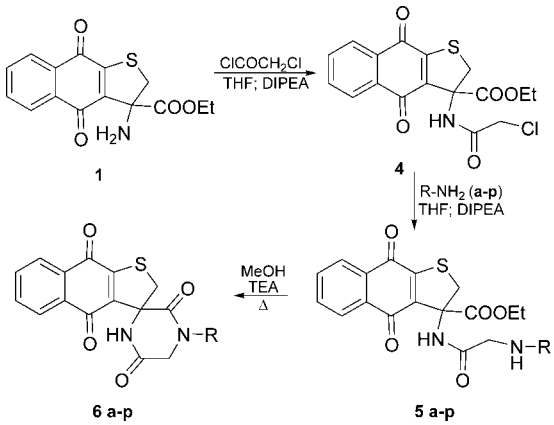

the 3-amino-3-(ethoxycarbonyl)-2,3-dihydrothieno[2,3-*b*]naphtho-4,9-dione system (**1**, DTNQ)[11] with *N*-Fmoc-Gly[a] and subsequent intramolecular lactamization, as described previously.[14]

The 4-substituted spiro-[(dihydropyrazine-2,5-dione)-6,3′-(2′,3′-dihydrothieno[2,3-*b*]-naphtho-4′,9′-dione)] derivatives were prepared via the route depicted in Scheme 1.

The condensation of 3-amino-3-ethoxycarbonyl-2,3-dihydrothieno[2,3-*b*]naphtho-4,9-dione (**1**, DTNQ) with chloroacetyl chloride in THF, using diisopropylethylamine as base, afforded the derivative 3-(2′-chloro)acetamide-3-ethoxycarbonyl-2,3-dihydrothieno[2,3-*b*]naphtho-4,9-dione (**4**) with 90% yield. Then, nucleophilic displacement of the chloride functionality with a variety of amine derivatives (**a**–**p**, Figure 2), in THF and diisopropylethylamine at reflux, readily provided the corresponding (2′-aminoalkyl *o*-aminoalkylsubstituted)acetamide analogues of general formula **5a**−**p**.

Under the above reaction conditions, the HPLC and ^{1}H NMR analysis of the crude reactions showed a partial cyclization, to a greater or lesser extent, of linear compounds. The complete lactamization of these derivatives in MeOH at reflux using TEA as base afforded the corresponding final 4-N-substituted spirodiketopiperazine derivatives (**6a**−**d**, **6i**−**p**) in 40–55% overall yields. Then these compounds were treated with a solution of hydrochloric acid in diethyl ether to provide the corresponding hydrochloride salts. This was found to both aid purification and provide an improved solubility profile for the biological assays. The final thioethyl (**6e**), thiopropyl (**6f**), aminoethyl (**6g**), and aminopropyl (**6h**) derivatives were obtained after S-Trt or NH-Boc deprotection using 20% TFA in dichloromethane in quantitative yields.

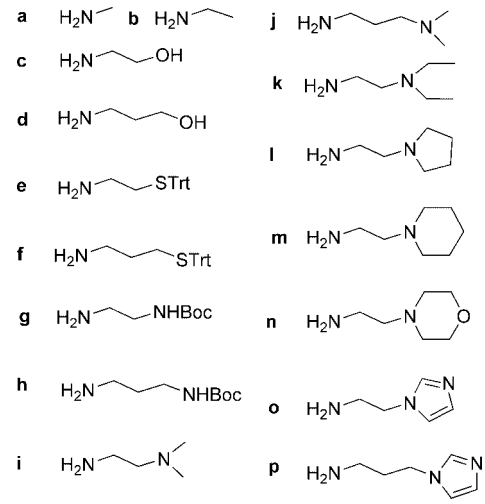

Figure 2. Structures of the amine derivatives used in this study.

Because the synthetic pathway used for the preparation of the starting DTNQ generates an asymmetric carbon (C-3) in this system,[11] the final compounds were obtained as racemic mixtures. To verify and evaluate the importance of the stereochemistry of this chiral center on the activity in this series of compounds, the synthesis of the enantiomerically pure compounds **3**, **6i**, and **6l** was performed starting from pure enantiomers of DTNQ. The racemic mixture of starting DTNQ (**1**) was resolved in the two corresponding enantiomers following the Evans method as reported previously.[13,16] Subsequently, reaction of enantiomers (+)-*S*-**1** and (−)-*R*-**1** with *N*-Fmoc-Gly[14] or (*N*,*N*-dimethyl)ethylenediamine and 2-pyrrolidinoethylamine, following the above general procedures gave the corresponding

[a] Abbreviations: Abbreviations used for amino acids follow the rules of the IUPAC-IUB Commission of Biochemical Nomenclature in *J. Biol. Chem.* 1972, *247*, 977–983. The following additional abbreviations are used: Boc, *tert*-butyloxycarbonyl; Trt, triphenylmethyl (trityl); DIPEA, *N*,*N*-diisopropylethylamine; FAB-MS, fast-atom bombardment mass spectrometry; Fmoc, 9-fluorenylmethoxycarbonyl; RP-HPLC, reversed-phase high performance liquid chromatography; STD, saturation transfer difference; TFA, trifluoroacetic acid; TLC, thin-layer chromatography.

Table 1. Cytotoxic Activity of Spiro[(dihydropirazin-2,5-dione)-6,3′-(2′,3′-dihydrothieno[2,3-*b*]naphtho-4′,9′-dione)] Derivatives (**3**) and 4-Substituted-spiro[(dihydropirazin-2,5-dione)-6,3′-(2′,3′-dihydrothieno[2,3-*b*]naphtho-4′,9′-dione)] Derivatives (**6a–p**)

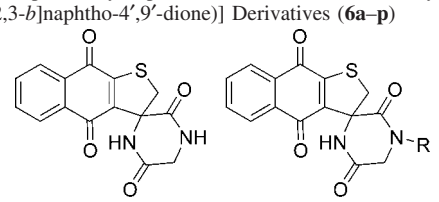

3 **6a-p**

compound	R	IC$_{50}$ (μM ± SD)[a] MCF-7[b]	SW 620[c]
3	H	0.041 ± 0.005	0.241 ± 0.043
(+)-3′*S*-**3**	H	0.049 ± 0.001	0.326 ± 0.010
(−)-3′*R*-**3**$^{-}$	H	0.046 ± 0.001	0.267 ± 0.008
6a	-CH_3	0.073 ± 0.005	0.381 ± 0.043
6b	-CH_2CH_3	0.141 ± 0.010	0.670 ± 0.043
6c	-$(CH_2)_2OH$	0.170 ± 0.005	0.350 ± 0.020
6d	-$(CH_2)_3OH$	0.420 ± 0.020	1.950 ± 0.020
6e	-$(CH_2)_2SH$	0.090 ± 0.003	0.250 ± 0.020
6f	-$(CH_2)_3SH$	0.380 ± 0.012	1.365 ± 0.020
6g[d]	-$(CH_2)_2NH_2$	0.047 ± 0.007	0.117 ± 0.009
6h[d]	-$(CH_2)_3NH_2$	0.299 ± 0.006	1.659 ± 0.292
6i[e]	-$(CH_2)_2N(CH_3)_2$	0.031 ± 0.012	0.112 ± 0.020
(+)-3′*S*-**6i**	-$(CH_2)_2N(CH_3)_2$	0.041 ± 0.008	0.170 ± 0.012
(−)-3′*R*-**6i**	-$(CH_2)_2N(CH_3)_2$	0.020 ± 0.008	0.100 ± 0.010
6j[e]	-$(CH_2)_3N(CH_3)_2$	0.139 ± 0.027	0.377 ± 0.073
6k[e]	-$(CH_2)_2N(CH_2CH_3)_2$	0.043 ± 0.012	0.123 ± 0.028
6l[e]	ethylpyrrolidine	0.040 ± 0.010	0.119 ± 0.005
(+)-3′*S*-**6l**	ethylpyrrolidine	0.056 ± 0.008	0.141 ± 0.007
(−)-3′*R*-**6l**	ethylpyrrolidine	0.030 ± 0.008	0.098 ± 0.002
6m[e]	ethylpiperidine	0.069 ± 0.020	0.198 ± 0.027
6n[e]	ethylmorpholine	0.050 ± 0.020	0.164 ± 0.027
6o[e]	ethylimidazole	0.116 ± 0.035	1.067 ± 0.139
6p[e]	propylimidazole	0.241 ± 0.035	1.423 ± 0.139
doxorubicin		0.022 ± 0.008	0.178 ± 0.003

[a] Data represent mean values (SD) for three independent determinations. [b] Human breast carcinoma cell line. [c] Human colon carcinoma cell line. [d] Evaluated as TFA salts. [e] Evaluated as HCl salts.

(+)-3′*S*-**3**, (−)-3′*R*-**3**, (+)-3′*S*-**6i**, (−)-3′*R*-**6i**, (+)-3′*S*-**6l**, and (−)-3′*R*-**6l** derivatives. The physicochemical properties and purity of the final compounds were assessed by TLC, LC-MS, analytical RP-HPLC, and NMR analysis.

In Vitro Cytotoxicity. The spirodiketopiperazine derivatives were examined for antiproliferative activity against the MCF-7 human breast carcinoma and SW 620 human colon carcinoma cell lines, and the IC$_{50}$ values obtained are summarized in Table 1. For comparative purposes, doxorubicin was also included in the assay. As shown in Table 1, nonsubstituted compound **3** showed a potent cytotoxic activity on the MCF-7 and SW 620 cell lines, being only 2-fold less potent than doxorubicin. The incorporation at position N-4 of small alkyl substituents such as methyl (**6a**) or ethyl (**6b**) was tolerated even with a loss in activity (2- and 3-folds, respectively), presumably due to the increasing lipophilic nature of the side chain. The most interesting results were obtained with the incorporation of a primary or tertiary amine to the end of the ethyl side chains. The spirodiketopiperazine derivatives **6g**, **6i**, and **6k** retained cytotoxic levels similar to those of doxorubicin on the MCF-7 human breast cell line, with IC$_{50}$ values of 47, 31, and 43 nM, respectively. These compounds were more active than doxorubicin on the SW 620 human colon cell line, with IC$_{50}$ values of 117, 112, and 123 nM, respectively.

The activity levels were also maintained with the replacing of the amino group with various nitrogen heterocycles. Thus, the derivatives containing pyrrolidin- (**6l**), piperidin- (**6m**), or morpholin-(**6n**) ethyl residues showed cytotoxic activity (IC$_{50}$) in the range 40–60 nM on the MCF-7 cell line. In addition, the pyrrolidin-derivative **6l** was the most active on the SW-620 (IC$_{50}$ = 119 nM). In general, the results listed in Table 1 indicate that only compounds possessing a positively charged amino group at physiological pH provide the best results regarding the cytotoxicity. In fact, congeners with a hydroxyl or thiol groups (compounds **6c**−**f**) were less potent compared to their primary and tertiary amine analogues. Compound **6o** containing an imidazole motif, was 3-fold less potent than compound **6l** (IC$_{50}$ = 116 vs 40 nM). In this case, we might suppose that the aromatic nature of the heterocyclic side chain, relatively rigid and more electron-rich when compared to the alkylcyclic pyrrolidine, is not well-tolerated in the molecular target.

The results in Table 1 showed other important SARs for this series of derivatives. First, the side-chain length, determined by the number of methylene groups separating the chromophore and the remote protonatable amine groups in the pendant arm, appears to have an important effect upon cytotoxicity. Thus, compounds containing a propyl carbon chain (**6d**, **6f**, **6 h**, **6j**, and **6p**) were 3–6-fold less potent than the corresponding analogues with an ethyl carbon chain. When these results were compared with those obtained for the previously reported spirohydantoine series[13] in which side chain length appears to have no effect upon cytotoxicity, it is clear that an increase of both the dimension and the flexibility of the spiro nucleus attached to the DTNQ chromophore (diketopiperazine vs hydantoine) limits the optimal side chain accommodation. Second, the relative configurations at the 3′-carbon have a weak influence on the cytotoxic activity of these compounds. Thus, while the enantiomers nonsubstituted *S*-**3** and *R*-**3** showed an activity similar to the corresponding racemic compound **3** (IC$_{50}$ = 49, 46, and 41 nM respectively), the pure 3′*R*-**6i** and 3′*R*-**6l** enantiomers (IC$_{50}$ = 20 and 30 nM, respectively) were only 2- and 1.7-fold more potent than the corresponding 3′*S* enantiomers (IC$_{50}$ = 41 and 56 nM, respectively) on the MCF-7 cell line. In addition, these compounds were more active than doxorubicin on the SW 620 cell line (IC$_{50}$ 100 and 98 vs 178 nM). The selectivity induced by the stereochemistry of C-3′ in these new 4-substituted spirodiketopiperazine derivatives was not as determinant as previously observed in the analogues of the 3-substituted-spiro[(dihydropyrazine-2,5-dione)-6,3′-(2′,3′-dihydrothieno[2,3-*b*] naphtho-4′,9′- dione)] series.[14]

To further determine the antitumor spectra and drug-resistance profile, compounds **3**, **6i**, and **6l** and their pure enantiomers 3′*S*-**3**, 3′*R*-**3**, 3′*S*-**6i**, 3′*R*-**6i**, 3′*S*-**6l**, and 3′*S*-**6l** were selected and screened against a panel of human tumor cell lines, including selected breast subline resistant to doxorubicin (MCF-7/Dx). As observed in Table 2, in the tested A549 (lung), HEK-293 (kidney), M14 (melanoma), and HeLa (cervical adenocarcinoma) human cell systems, all of the compounds showed marked cytotoxic potency at submicromolar concentrations. The compound **6l** and its pure enantiomers resulted in the most active compounds against A549 (lung) and M14 (melanoma), with IC$_{50}$ values in the range 0.18–0.24 μM. The **6i** derivatives also showed potent activity against HEK-293 (kidney) cell line (IC$_{50}$ = 0.20 μM), while they were less potent on A549 (lung) and M-14 (melanoma) cell lines (IC$_{50}$ = 0.45 and 0.34 μM, respectively).

The data showed a remarkable activity of these compounds against cell lines generally highly resistant to treatment with doxorubicin. In fact, these derivatives were 2- to 4-fold more potent than doxorubicin on the M-14 (melanoma) and HeLa (cervical adenocarcinoma) human cell systems. In addition, the doxorubicin resistant MCF-7/Dx cell line exhibited a low level

Table 2. Inhibition of Multiple Human Tumor Cell Lines by Selected Compounds

	IC_{50} (μM ± SD)[a]					
compound	A549 lung	HEK-293 kidney	M-14 melanoma	HeLa cervical	MCF-7 ovarian	MCF-7/Dx
3	0.640 ± 0.030	0.410 ± 0.020	0.539 ± 0.020	0.510 ± 0.010	0.041 ± 0.005	0.240 ± 0.009
3′*S*-**3**	0.690 ± 0.04	0.420 ± 0.030	0.563 ± 0.010	0.510 ± 0.020	0.049 ± 0.001	0.248 ± 0.010
3′*R*3⁻	0.630 ± 0.05	0.398 ± 0.030	0.530 ± 0.010	0.506 ± 0.010	0.046 ± 0.001	0.237 ± 0.010
6i	0.464 ± 0.02	0.206 ± 0.01	0.341 ± 0.010	0.398 ± 0.030	0.031 ± 0.012	0.109 ± 0.020
3′*S*-**6i**	0.454 ± 0.05	0.220 ± 0.03	0.356 ± 0.030	0.400 ± 0.040	0.041 ± 0.008	0.122 ± 0.020
3′*R*-**6i**	0.432 ± 0.03	0.196 ± 0.03	0.330 ± 0.010	0.310 ± 0.020	0.020 ± 0.008	0.080 ± 0.020
6l	0.190 ± 0.008	0.211 ± 0.01	0.237 ± 0.012	0.445 ± 0.020	0.040 ± 0.010	0.236 ± 0.020
3′*S*-**6l**	0.205 ± 0.020	0.220 ± 0.029	0.260 ± 0.030	0.460 ± 0.030	0.056 ± 0.008	0.240 ± 0.020
3′*R*-**6l**	0.180 ± 0.020	0.195 ± 0.013	0.230 ± 0.030	0.401 ± 0.030	0.030 ± 0.008	0.130 ± 0.020
doxorubicin	0.031 ± 0.008	0.064 ± 0.010	0.820 ± 0.100	1.009 ± 0.070	0.022 ± 0.008	5.300 ± 0.40

[a] Data represent mean values (SD) for three independent determinations.

Table 3. Effect of Doxorubicin and **6i** and **6l** Derivatives on CaCo-2 Cell Growth[a]

	% cell proliferation					
treatment (h)	control	doxorubicin	3′*R*-**6i**	3′*S*-**6i**	3′*R*-**6l**	3′*S*-**6l**
24	100 ± 9	60 ± 8	46 ± 7	59 ± 6	56 ± 8	76 ± 5
48	100 ± 2	100 ± 5	60 ± 7	80 ± 4	72 ± 5	100 ± 5
72	100 ± 1	130 ± 7	36 ± 3	110 ± 1	46 ± 1	143 ± 1

[a] CaCo-2 cells were cultured in DMEM without serum and treated with 50 nM doxorubicin, 3′*R*-**6i**, 3′*S*-**6i**, 3′*R*-**6l**, and 3′*S*-**6l**. After 24, 48, and 72 h, the cell proliferation was determined through CyQuant cell proliferation assay Kit (Invitrogen, Milan) with dye fluorescence measurement (480 nm exc. and 520 nm em.). The culture medium with all derivatives was changed at 48 h. Cell proliferation was expressed in percentage of proliferation compared with the control. All data are the mean ± SD of three experiments.

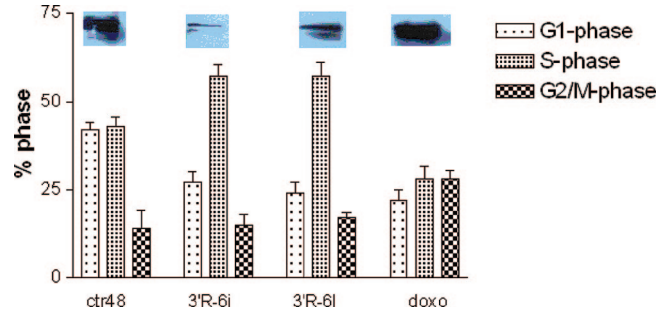

Figure 3. Effects of doxorubicin, 3′*R*-**6i**, and 3′*R*-**6l** on the distribution of cell populations data represent the percentage of cells in each cell cellular cycle phases. For 3′*R*-**6i**: G1, 27.0%; S, 57.0%; G2/M, 15.0%; 3′*R*-**6l**: G1, 24.0%; S, 57.0%; G2/M, 17.0%; **doxo**: G1, 22.0%; S, 28.0%; G2/M, 28.0%. In the inset was reported the Western blot expression of cyclin A in the control and induced by 3′*R*-**6i**, 3′*R*-**6l**, and doxorubicin.

of cross-resistance to all the tested compounds (resistance indexes were in the range 3–4).

On the other hand, we analyzed the possibility that this class of compounds could inhibit the activity of topoisomerase II (topo II).[17] However, compounds **3**, **6i**, and **6l** did not inhibit topo II catalytic activity at a concentration of 50 μM (data not showed). These results are in agreement with the low level of cross-resistance observed on cell lines resistant to doxorubicin and suggest that this series of compounds has a distinct mechanism of action.

Cell Cycle Effects. To investigate the cytotoxic effects of these derivatives in more detail, we examined the effects on growth and cell cycle progression in CaCo-2 cell line.[18] Doxorubicin was added to this study for comparative purpose.

CaCo-2 cell proliferation was measured at 24, 48, and 72 h after each treatment (see Experimental Section) at 50 nM concentration. To investigate if we have obtained a drug-resistant cell population, we have changed the culture medium with all compounds tested at 48 h. According to the results summarized in Table 3, a significant difference between the CaCo-2 cell line treated with the *R*- and *S*-enantiomers of **6i** and **6l** was observed. Thus, a net decrease in the total number of cells and an accumulation of cell floating in the culture medium was observed only in the case of CaCo-2 cells incubated for 72 h with 3′*R*-**6i** and 3′*R*-**6l** derivatives (64 and 54% of cell death, respectively). At the same time and analogously to doxorubicin, the corresponding 3′*S*-**6i** and 3′*S*-**6l** isomers induced resistance to CaCo-2 cells and were not antiproliferatives (cell proliferation >100%).

In an effort to elucidate whether cell cycle perturbation was related to the inhibition of cell growth, the percentage of CaCo-2 cells in G1, S, and G2/M phases was analyzed after 48 h of treatment with 50 nM concentration of 3′*R*-**6i**, 3′*R*-**6l**, and doxorubicin (Figure 3). Under these conditions, the control cells were in the G-1 phase 42%, S phase 43%, and G2/M phase 14%. The treatment with our derivatives resulted in accumulation of cells in the S phase, while concomitantly the G1 populations decreased. About 57% of the CaCo-2 cells were arrested at the S phase, whereas at the same concentration, the doxorubicin induced an increase of percentage in G2/M phase (28%).

On the other hand and as showed in the inset of Figure 3, at 50 nM concentration, the 3′*R*-**6i** and 3′*R*-**6l** derivatives induced a significant decrease of cyclin A expression,[19] indicating that the cell cycle progression of cells in the S phase was markedly delayed and the cells do not transient to the G_2/M phase. At the same time, doxorubicin did not show any inhibitor activity on cyclin expression. These preliminary results suggested that the inhibition of cell proliferation was induced, at least in part, by the cells exposure to compounds 3′*R*-**6i** and 3′*R*-**6l** in the S phase and by the subsequent delay of cell cycle progression in responsive cells.

DNA Binding Properties. STD NMR. Two representative compounds, that is, **6i** and **6p**, were tested to see if they interact with DNA, using the saturation transfer difference (STD) NMR[20,21] technique. STD NMR is a technique that can be used to characterize and identify binding. This technique has become increasingly important as a tool in the investigation of biomolecular recognition phenomena. The STD NMR technique is a method of epitope mapping and ligand screening by NMR spectroscopy. Resonances of the macromolecule are selectively saturated, and in a binding ligand, enhancements are observed in the difference (STD NMR) spectrum resulting from subtraction of this spectrum from a reference spectrum in which the macromolecule is not saturated. Protons of the ligand which are in close contact with the macromolecule can easily be identified from the STD NMR spectrum, because they are saturated to the highest degree. They should have stronger STD, and this allows direct observation of areas of the ligand that

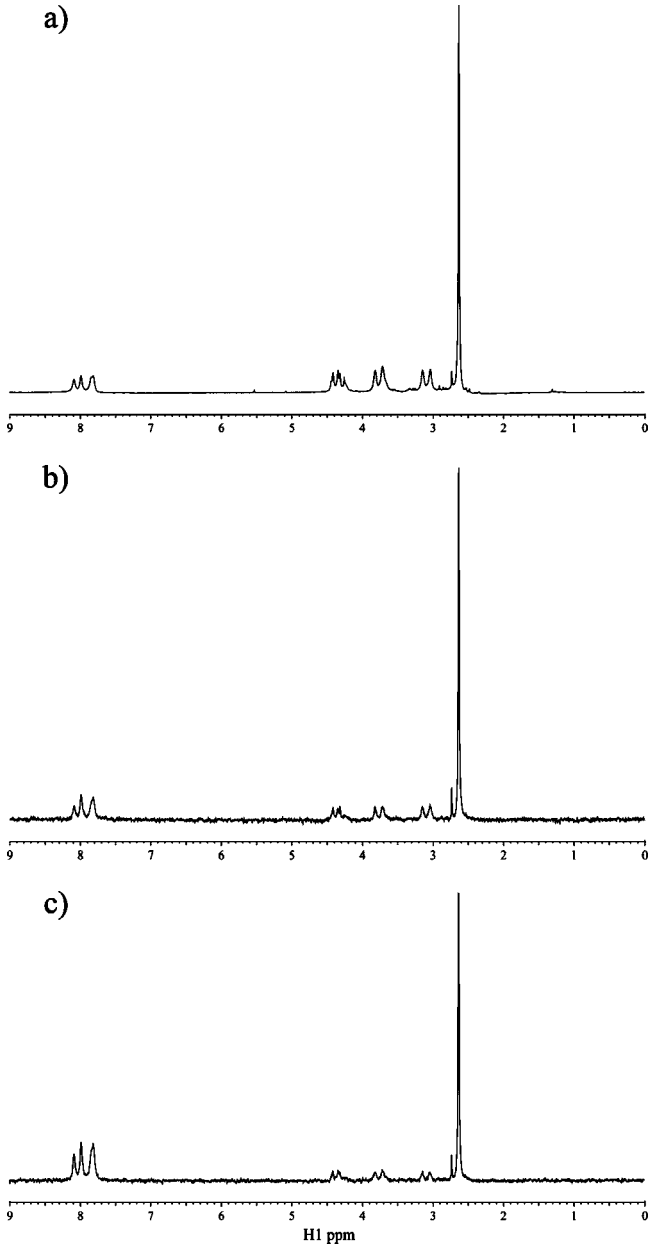

Figure 4. 1D proton spectrum of **6i** (1 mM)/DNA (50 μM) complex (a). The corresponding STD NMR spectra recorded upon saturation at –1 ppm (b) and 10 ppm (c). The last two spectra were plotted with the same noise level.

comprises the epitope. Figure 4a shows the ^{1}H NMR spectrum of **6i** in the presence of poly(dG-dC)·poly(dG-dC) copolymer as DNA target. Figure 4b,c shows the corresponding STD spectra upon irradiation at −1 ppm and 10 ppm, respectively. All the proton resonances of **6i** were observed in both the STD spectra, demonstrating that **6i**/DNA interactions did occur.

Furthermore, we applied the so-called DF-STD (differential frequency STD) spectroscopy,[22] to study the binding modes of our ligands with the DNA. The method allows the discrimination of base-pair intercalators, minor-groove, and external binders. The approach is based on the comparison of two parallel sets of STD experiments performed under the same experimental conditions, in which saturation is centered either in the aromatic or in the low-field aliphatic spectral regions. Due to the anisotropy in the efficiency of saturation diffusion along the vertical and horizontal dimensions of helical DNA, a ligand making proximate contacts with aromatic base protons, such as an intercalator sandwiched by consecutive base pairs, would receive more saturation upon irradiation of DNA aromatic protons rather than irradiation of deoxyribose protons. Conversely, an external ligand presenting the majority of its binding surface in contact with the DNA phosphodiester backbone should be more affected by irradiation in the deoxyribose region rather than by irradiation in the DNA aromatic region. The "binding mode index" (BMI), a numerical parameter that expresses the relative sensitivity of ligand protons to the perturbation arising from each type of saturation (that is, base versus sugar/backbone saturation) were used. Three BMI ranges could be extrapolated: 0 < BMI < 0.50 for external (nonspecific) electrostatic backbone binding; 0.90 < BMI < 1.10 for minor groove binding; and 1.20 (0.90) < BMI < 1.50 for base-pair intercalation.

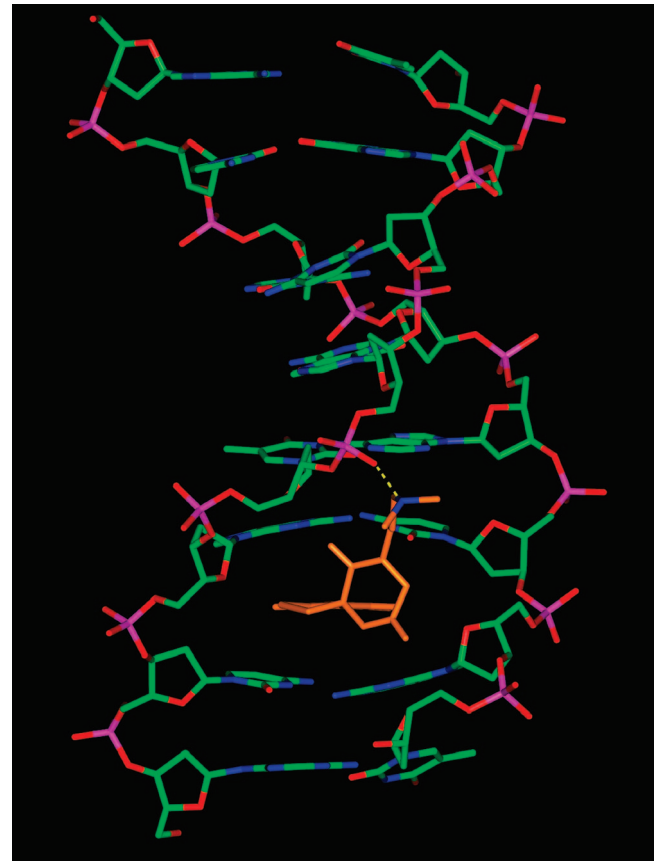

Figure 5. Energy-minimized structure of the complex **6i**/[d(ACGTACGT)]$_2$.

DF-STD analysis of compound **6i** gave different BMI values: BMI = 0.34, for the methyl signal; BMI = 0.68 for the ethylene signals; and BMI = 1.42 for the aromatic signals. This result can be explained assuming two different DNA binding modes for **6i**. An intercalative mode of binding is sustained by its tricyclic planar core, and an external backbone binding can be attributed to its ethylamine side chain. This is similar to that observed for compounds of the series III.[14] We performed the same STD NMR analysis also on compound **6p**, which bears a propylimidazole side chain and shows a reduced cytotoxic activity compared to **6i**. Analysis of compound **6p** demonstrated that this compound also binds to DNA with similar DF-STD profile as **6i** ($BMI_{imidazole}$ = 0.98, BMI_{propyl} = 0.65, and $BMI_{naphthoquinone}$ = 1.22), indicating analogous binding mode for these two compounds. Figure 5 shows a model of the **6i**/DNA interaction. The model was obtained starting from the **3′**/DNA complex derived in our previous work,[14] followed by extended

minimization. Apart from the stabilizing interactions already found in the **3′**/DNA complex (hydrogen bonds and $\pi-\pi$ stacking forces),[14] **6i**/DNA complex is also stabilized by an electrostatic interaction between the (dimethyl)amino group of **6i** and a phosphate group of the DNA, as evidenced in Figure 5.

Conclusions

The results herein described demonstrated that chemical modification at the diketopiperazine domain attached to the DTNQ planar system was an effective approach to optimize the activity profiles of these derivatives. Several compounds, carrying a distal protonated ethyl amine moiety, showed a similar or greater cytotoxic potency than doxorubicin against the human breast (MCF-7) and colon (SW 620) tumor cell lines. In particular, compounds **6i** and **6l** in both racemic and pure enantiomeric forms showed a high efficacy in cell lines resistant to doxorubicin (MCF-7/Dx) and in cell lines, which were highly resistant to treatment with doxorubicin, such as HEK-293 (kidney), M-14 (melanoma), and HeLa (cervical adenocarcinoma) human cell lines. Preliminary studies on cell cycle progression in CaCo-2 cell line showed that the 3′*R*-**6i** and 3′*R*-**6l** derivatives markedly prolonged the S phase of the cell cycle inducing delay of cell cycle progression in responsive cells and cellular proliferation inhibition. All these data revealed significant differences in the cytotoxic behavior of these compounds compared to doxorubicin. STD-NMR spectroscopy investigation performed on compounds **6i** and **6p** demonstrated that they interact with DNA with a dual binding mode: intercalative for the tricyclic planar core and external considering the side-chain moiety. Further experiments aimed at defining the target and the mechanisms of the growth-inhibitory effect shown by these molecules are currently underway.

Experimental Section

Chemistry. Reagents, starting materials, and solvents were purchased from commercial suppliers and used as received. Analytical TLC was performed on a 0.25 mm layer of silica gel 60 F_{254} (Merck). Silica gel 60 (300–400 mesh, Merck) was used for flash chromatography. Melting points were taken on a Kofler apparatus and are uncorrected. Optical rotations were determined with a Perkin-Elmer-241 MC polarimeter. ^{1}H NMR and ^{13}C NMR spectra were recorded with a Bruker-500 spectrometer, operating at 500 and 125 MHz, respectively. Chemical shifts are reported in δ values (ppm) relative to internal Me_4Si, and *J* values are reported in Hertz (Hz). Mass spectra were obtained using a FAB-MS spectrometer. Analytical RP-HPLC was performed on a Vydac C-18 (25−0.46 cm) column, using a tunable UV detector set at 215 nm. Elution was performed with a linear gradient from 10 to 60% of acetonitrile in 0.1% aqueous TFA over 55 min at a flow rate of 1 mL/min. The 3-amino-3-ethoxycarbonyl-2,3-dihydrothieno[2,3-*b*]naphtho-4,9-dione system (DTNQ) and the spiro[(dihydropyrazine-2,5-dione)-6,3′-(2′,3′-dihydrothieno [2,3-*b*]naphtho-4′,9′-dione)] (**3**) were synthesized according to the procedure previously described.[11,14] The pure enantiomers (+)-*S*- and (−)-*R*-DTNQ were obtained following the Evans method as is previously reported.[11,13,16]

3-(2′-Chloro)acetamide-3-ethoxycarbonyl-2,3-dihydrothieno[2,3-*b*]naphtho-4,9-dione (4). DTNQ (2 g, 6.6 mmol) was dissolved in THF, and chloroacetyl chloride (0.9 g, 8 mmol) and TEA (2.2 equiv) were added to the solution. The mixture reaction was stirred at room temperature for 1 h after which chloroform and water were added. The organic layer was washed with water and dried. Concentration of the chloroform phase gave the crude product, which was purified by column chromatography, using chloroform as eluent, to obtain the title product as a yellow solid (2.2 g, 89%), mp 109–111 °C. ^{1}H NMR (500 MHz, $CDCl_3$) δ 1.23 (m, 3H, CH_3); 3.36 (d, 1H, *J* = 12.8 Hz, H-2); 4.05 (m, 2H, C*H*$_2$); 4.46 (d, 1H, H-2′); 6.81 (s, 1H, NH); 7.73–7.77 (m, 2H, H-6 and H-7); 8.00 (d, 1H, *J* = 8.0 Hz, H-8); 8.10 (d, 1H, *J* = 7.6 Hz, H-5). MS [M^+] calcd for $C_{17}H_{14}NO_5SCl$, 379.03; found, 379.12.

General Procedure for the Synthesis of the 4-Alkyl(alkyl-substituted) Spiro[(dihydropirazin-2,5-dione)-6,3′-(2′,3′-dihydrothieno[2,3-*b*]naphtho-4′,9′-dione)] Derivatives (6a−p). To a solution of 3-(2′-chloro)acetamide-3-ethoxycarbonyl-2,3-dihydrothieno[2,3-*b*]naphtho-4,9-dione (150 mg, 0.4 mmol) in THF (20 mL) were added the corresponding amine (1.1 equiv): methylamine, N-Boc-ethylendiamine, N-Boc-propylendiamine, ethanolamine, propanolamine, 2-(tritylthio)ethanamine, 3-(tritylthio)propylamine, *N*,*N*-dimethylethylamine, *N*,*N*-dimethyl-1,3-propanediamine, *N*,*N*-diethylethylendiamine, 2-(pyrrolidin-1-yl)ethanamine, 2-(piperidin-1-yl)ethanamine, 2-morpholinoethanamine, 2-(imidazol-1-yl)ethanamine, or 3-(imidazol-1-yl)propanamine and DIPEA (0.3 mL, 2 mmol). After stirring at reflux temperature for 1–3 h, the solvent was evaporated and the residue was dissolved into methanol (20 mL) and TEA (0.15 mL, 1 mmol). The reaction mixture was stirring for 3–6 h at reflux temperature, then neutralized with 1 N HCl, and diluted with Cl_3CH. The organic extract was washed with 10% $NaHCO_3$ and water, dried over Na_2SO_4, and evaporated to dryness. Flash chromatography of the residues, using $CHCl_3$ or a gradient of 0–20% MeOH in $CHCl_3$ as eluent system, yielded, in each case, the correspondent spirohydantoin derivatives.

General Procedure for Removal of the Side Chain Protecting Group. A solution of Boc or Trt side chain protected derivatives (**6′e**−**h**, 0.03–0.05 mmol) in dichloromethane (10 mL) was treated with trifluoroacetic acid (2 mL) and stirred at room temperature for 3–6 h. After evaporation to dryness, the treatment of residue with dichloromethane and diethyl ether yielded the corresponding final compounds **6e**−**h**. The purity of all these compounds was assessed as being >98% using HPLC, microanalyses, and NMR spectroscopy.

Data for 4-Methylspiro[(dihydropirazin-2,5-dione)-6,3′-(2′,3′-dihydrothieno[2,3-*b*]naphtho-4′,9′-dione)] (6a). Yellow solid (54%), mp 135–136 °C. HPLC t_R 17.4 min. ^{1}H NMR (500 MHz, $CDCl_3$) δ 3.09 (s, 3H, CH_3); 3.36 (d, 1H, *J* = 12.8 Hz, H-2′); 4.04 (d, 1H, *J* = 17.6 Hz, Ha-3); 4.45 (d, 1H, Hb-3); 4.46 (d, 1H, H-2″); 6.81 (s, 1H, NH); 7.73–7.77 (m, 2H, H-6′ and H-7′); 8.00 (d, 1H, *J* = 8.0 Hz, H-8′); 8.10 (d, 1H, *J* = 7.6 Hz, H-5). FAB-MS *m*/*z* calcd for $C_{16}H_{12}N_2O_4S$, 328.05; found, 328.21.

Data for 4-Ethylspiro[(dihydropirazin-2,5-dione)-6,3′-(2′,3′-dihydrothieno[2,3-*b*] naphtho-4′,9′-dione)] (6b). Yellow solid (53%), mp 143–145 °C. HPLC t_R 17.9 min. ^{1}H NMR (500 MHz, $CDCl_3$) δ 1.38 (m, 3H, C*H*$_3$); 3.33 (d, 1H, *J* = 12.7 Hz, H-2′); 3.61–3.63 (m, 2H, C*H*$_2$); 4.00 (d, 1H, *J* = 17.7 Hz, Ha-3); 4.24 (d, 1H, Hb-3); 4.43 (d, 1H, H-2″); 6.65 (s, 1H, NH); 7.72–7.75 (m, 2H, H-6′ and H-7′); 7.98 (d, 1H, *J* = 7.7 Hz, H-8′); 8.09 (d, 1H, *J* = 7.2 Hz, H-5). FAB-MS *m*/*z* calcd for $C_{17}H_{14}N_2O_4S$, 342.07; found, 342.30.

Data for 4-(2-Hydroxyethyl)spiro[(dihydropirazin-2,5-dione)-6,3′-(2′,3′-dihydrothieno[2,3-*b*]naphtho-4′,9′-dione)] (6c). Yellow solid (48%), mp 183 °C (dec). HPLC t_R 18.9 min. ^{1}H NMR (500 MHz, $CDCl_3$) δ 2.92 (s, 1H, O*H*); 3.42 (d, 1H, *J* = 12.6 Hz, H-2′); 3.76–3.78 (m, 2H, C*H*$_2$); 3.87–3.89 (m, 2H, C*H*$_2$); 4.05 (d, 1H, *J* = 17.7 Hz, Ha-3); 4.21 (d, 1H, Hb-3); 4.39 (d, 1H, H-2″); 6.16 (s, 1H, NH); 7.74–7.77 (m, 2H, H-6′ and H-7′); 8.03 (d, 1H, *J* = 7.7 Hz, H-8′); 8.10 (d, d, 1H, *J* = 7.2 Hz, H-5). HPLC t_R 18.6 min. FAB-MS *m*/*z* calcd for $C_{17}H_{14}N_2O_5S$, 358.06; found, 358.31.

Data for 4-(3-Hydroxypropyl)spiro[(dihydropirazin-2,5-dione)-6,3′-(2′,3′-dihydrothieno[2,3-*b*]naphtho-4′,9′-dione)] (6d). Yellow solid (51%), mp 191 °C (dec). HPLC t_R 19.3 min. ^{1}H NMR (500 MHz, $CDCl_3$) δ 1.21–1.24 (m, 2H, C*H*$_2$); 1.90–1.93 (m, 2H, C*H*$_2$); 3.39 (d, 1H, *J* = 12.7 Hz, H-2′); 3.72–3.76 (m, 2H, C*H*$_2$); 4.00 (d, 1H, *J* = 17.7 Hz, Ha-3); 4.24 (d, 1H, Hb-3); 4.39 (d, 1H, H-2″); 6.97 (s, 1H, NH); 7.69–7.74 (m, 2H, H-6′ and H-7′); 7.98 (d, 1H, *J* = 7.8 Hz, H-8′); 8.04 (d, 1H, *J* = 7.3 Hz, H-5). HPLC t_R 19.4 min. FAB-MS *m*/*z* calcd for $C_{18}H_{16}N_2O_5S$, 372.08; found, 372.29.

Data for 4-(2-Thioethyl)spiro[(dihydropirazin-2,5-dione)-6,3′-(2′,3′-dihydrothieno[2,3-*b*]naphtho-4′,9′-dione)] (6e). Yellow solid (43%), mp 181–183 °C. HPLC t_R 20.4 min. ^{1}H NMR (500 MHz, $CDCl_3$) δ 2.76–2.78 (m, 2H, CH_2); 3.43 (d, 1H, J = 12.6 Hz, H-2′); 3.67–3.69 (m, 2H, CH_2); 4.04 (d, 1H, J = 17.7 Hz, Ha-3); 4.26 (d, 1H, Hb-3); 4.40 (d, 1H, H-2″); 6.72 (s, 1H, NH); 7.72–7.75 (m, 2H, H-6′ and H-7′); 7.98 (d, 1H, J = 7.7 Hz, H-8′); 8.09 (d, d, 1H, J = 7.2 Hz, H-5). HPLC t_R 18.6 min. FAB-MS *m*/*z* calcd for $C_{17}H_{14}N_2O_4S_2$, 374.04; found, 374.28.

Data for 4-(3-Thiopropyl)spiro[(dihydropirazin-2,5-dione)-6,3′-(2′,3′-dihydrothieno[2,3-*b*]naphtho-4′,9′-dione)] (6f). Yellow solid (45%), mp 199–200 °C. HPLC t_R 20.9 min. ^{1}H NMR (500 MHz, $CDCl_3$) δ 1.61–1.63 (m, 2H, CH_2); 2.62–2.64 (m, 2H, CH_2); 3.35 (d, 1H, J = 12.7 Hz, H-2′); 3.41–3.44 (m, 2H, CH_2); 3.98 (d, 1H, J = 17.7 Hz, Ha-3); 4.20 (d, 1H, Hb-3); 4.36 (d, 1H, H-2″); 6.77 (s, 1H, NH); 7.71–7.75 (m, 2H, H-6′ and H-7′); 8.01 (d, 1H, J = 7.8 Hz, H-8′); 8.06 (d, 1H, J = 7.3 Hz, H-5). HPLC t_R 19.4 min. FAB-MS *m*/*z* calcd for $C_{18}H_{16}N_2O_4S_2$, 388.05; found, 388.33.

Data for 4-(2-Amino)ethylspiro[(dihydropirazin-2,5-dione)-6,3′-(2′,3′-dihydrothieno[2,3-*b*]naphtho-4′,9′-dione)] Trifluoroacetate (6g). Yellow solid (46%), mp 184–186 °C. HPLC t_R 19.4 min. ^{1}H NMR (500 MHz, CD_3OD) δ 3.05–3.08 (m, 1H, CH_2); 3.37 (d, 1H, J = 12.8 Hz, H-2′); 3.44–3.47 (m, 1H, CH_2); 3.51 (d, 1H, H-2″); 3.85–3.89 (m, 1H, CH_2); 4.09 (d, 1H, J = 17.5 Hz, Ha-3); 4.36 (d, 1H, Hb-3); 7.73–7.77 (m, 2H, H-6′ and H-7′); 8.00 (d, 1H, J = 7.8 Hz, H-8′); 8.09 (d, 1H, J = 7.2 Hz, H-5′). HPLC t_R 19.4 min. FAB-MS *m*/*z* calcd for $C_{17}H_{15}N_3O_4S\cdot CF_3COOH$, 471.07; found, 471.39.

Data for 4-(3-Amino)propylspiro[(dihydropirazin-2,5-dione)-6,3′-(2′,3′-dihydrothieno [2,3-*b*]naphtho-4′,9′-dione)] Trifluoroacetate (6 h). Yellow solid (50%), mp 213–214. HPLC t_R 19.9 min. ^{1}H NMR (500 MHz, CD_3OD) δ 1.95–1.97 (m, 2H, CH_2); 3.03–3.05 (m, 1H, CH_2); 3.22–3.25 (m, 2H, CH_2); 3.38 (d, 1H, J = 12.8 Hz, H-2′); 3.51 (d, 1H, H-2″); 3.81–3.83 (m, 1H, CH_2); 3.91 (d, 1H, J = 17.5 Hz, H-3a); 4.32 (d, 1H, H-3b); 7.74–7.76 (m, 2H, H-6′ and H-7′); 8.05 (d, 1H, H-8′); 8.10 (d, 1H, H-5′). HPLC t_R 19.4 min. FAB-MS *m*/*z* calcd for $C_{18}H_{17}N_3O_4S\cdot CF_3COOH$, 485.09; found, 485.42.

Data for 4-[(2-*N*,*N*-Dimethyl)amino]ethylspiro[(dihydropirazin-2,5-dione)-6,3′-(2′,3′-dihydrothieno[2,3-*b*]naphtho-4′,9′-dione)] Hydrochloride (6i). Yellow solid (50%), mp 219–221 °C. HPLC t_R 16.8 min. ^{1}H NMR (500 MHz, CD_3OD) δ 2.30 (s, 6H, N−CH_3); 2.48–2.51 (m, 1H, CH_2); 2.64–2.67 (m, 1H, CH_2); 3.38 (d, 1H, J = 12.8 Hz, H-2′); 3.59–3.65 (m, 3H, CH_2, H-2″); 4.16 (d, 1H, J = 17.4 Hz, H-3a); 4.41 (d, 1H, H-3b); 7.73–7.77 (m, 2H, H-6′ and H-7′); 8.00 (d, 1H, J = 7.8 Hz, 8′-H); 8.09 (d, 1H, J = 7.2 Hz, 5′-H). ^{1}H NMR (500 MHz, D_2O) δ 2.82 (s, 6H, N−CH_3); 3.41–3.44 (m, 2H, CH_2); 3.71 (d, 1H, J = 12.8 Hz, H-2′); 3.84–3.87 (m, 1H, CH_2); 3.99–4.01 (m, 1H, CH_2); 4.19 (d, 1H, H-2″); 4.31 (d, 1H, J = 17.4 Hz, H-3a); 4.41 (d, 1H, H-3b); 7.83–7.87 (m, 2H, H-6′ and H-7′); 8.02 (d, 1H, J = 6.2 Hz, H-8′); 8.09 (d, 1H, J = 7.2 Hz, H-5′). FAB-MS *m*/*z* calcd for $C_{19}H_{19}N_3O_4S\cdot HCl$, 421.08; found, 421.28.

The pure enantiomers (+)-3′*S*-**6i** and (−)-3′*R*-**6i** were prepared from the corresponding (+)-*S*- and (−)-*R*-DTNQ and *N*,*N*-diethylethylendiamine following the general procedure indicated above. Data for 3′*S*-**6i**: $[\alpha]^D_{20}$ = +28.8° (*c* 1.2, MeOH); mp 220–221 °C. Data for 3′*R*-**6i**: $[\alpha]^D_{20}$ = −28.5° (*c* 1.1, MeOH); mp 219–221 °C.

Data for 4-[3-(*N*,*N*-Dimethyl)amino]propylspiro[(dihydropirazin-2,5-dione)-6,3′-(2′,3′-dihydro thieno[2,3-*b*]naphtho-4′,9′-dione) Hydrochloride (6j). Yellow solid (48%), mp 236–238 °C. HPLC t_R 17.2 min. ^{1}H NMR (500 MHz, CD_3OD) δ 2.37–2.39 (m, 2H, CH_2); 2.89 (s, 6H, N−CH_3); 3.31–3.34 (m, 3H, CH_2); 3.59 (d, 1H, J = 12.8 Hz, H-2′); 3.78 (d, 1H, H-2″); 3.98–4.00 (m, 1H, CH_2); 4.20 (d, 1H, J = 17.7 Hz, H-3a); 4.38 (d, 1H, H-3b); 7.83–7.86 (m, 2H, H-6′ and H-7′); 8.05 (d, 1H, J = 7.8 Hz, H-8′); 8.11 (d, 1H, J = 7.3 Hz, H-5′). HPLC *t*R 19.4 min. FAB-MS *m*/*z* calcd for $C_{20}H_{21}N_3O_4S\cdot HCl$, 435.10; found, 435.37.

Data for 4-[(2-*N*,*N*-Diethyl)amino]ethylspiro[(dihydropirazin-2,5-dione)-6,3′-(2′,3′-dihydrothieno[2,3-*b*]naphtho-4′,9′-dione)] Hydrochloride (6k). Yellow solid (50%), mp 240–241. HPLC t_R 17.7 min. ^{1}H NMR (500 MHz, CD_3OD) δ 1.31–1.35 (m, 6H, CH_3); 3.14–3.17 (m, 1H, CH_2); 3.32–3.40 (m, 4H, CH_2); 3.49–3.51 (m, 1H, CH_2); 3.55 (d, 1H, J = 12.8 Hz, H-2′); 3.62–3.65 (m, 2H, CH_2); 3.81 (d, 1H, H-2″); 3.97–3.99 (m, 1H, CH_2); 4.20 (d, 1H, J = 17.2 Hz, H-3a); 4.44 (d, 1H, H-3b); 7.80–7.86 (m, 2H, H-6′ and H-7′); 8.05 (d, 1H, J = 7.8 Hz, H-8′); 8.10 (d, 1H, J = 7.3 Hz, H-5′). HPLC t_R 19.4 min. FAB-MS *m*/*z* calcd for $C_{21}H_{23}N_3O_4S\cdot HCl$, 449.12; found, 449.41.

Data for 4-(2-Pyrrolydin)ethyl-spiro[(dihydropirazin-2,5-dione)-6,3′-(2′,3′-dihydrothieno[2,3-*b*]naphtho-4′,9′-dione) Hydrochloride (6l). Yellow solid (46%), mp 208–209 °C. HPLC t_R 16.7 min. ^{1}H NMR (500 MHz, CD_3OD) δ 1.60–1.64 (m, 4H, CH_2); 2.72–2.76 (m, 4H, CH_2); 3.05–3.06 (m, 2H, CH_2); 3.41 (d, 1H, J = 12.8 Hz, H-2′); 3.59 (d, 1H, H-2″); 3.62–3.64 (m, 1H, CH_2); 3.79–3.81 (m, 1H, CH_2); 4.20 (d, 1H, J = 17.6 Hz, H-3a); 4.39 (d, 1H, H-3b); 7.74–7.79 (m, 2H, H-6′ and H-7′); 8.00 (d, 1H, J = 7.7 Hz, H-8′); 8.09 (d, 1H, J = 7.2 Hz, H-5′). FAB-MS *m*/*z* calcd for $C_{21}H_{21}N_3O_4S\cdot HCl$, 447.10; found, 447.32.

The pure enantiomers (+)-3′*S*-**6l** and (−)-3′*R*-**6l** were prepared from the corresponding (+)- and (−)-DTNQ and 2-(pyrrolidin-1-yl)ethanamine following the general procedure indicated above. Data for 3′*S*-**7l**: $[\alpha]^D_{20}$ = +21.3° (*c* 1.3, MeOH); mp 209–210 °C. Data for 3′*R*-**7l**: $[\alpha]^D_{20}$ = −21.2° (*c* 1.0, MeOH); mp 209–210 °C.

Data for 4-(2-Piperidin)ethyl-spiro[(dihydropirazin-2,5-dione)-6,3′-(2′,3′-dihydrothieno [2,3-*b*]naphtho-4′,9′-dione) Hydrochloride (6m). Yellow solid (50%), mp 238–240. HPLC t_R 17.2 min. ^{1}H NMR (500 MHz, CD_3OD) δ 1.58–1.63 (m, 6H, CH_2); 2.30–2.33 (m, 4H, CH_2); 3.05–3.09 (m, 2H, CH_2); 3.35 (d, 1H, J = 12.7 Hz, H-2′); 3.51–3.54 (m, 2H, CH_2, H-2″); 3.69–3.71 (m, 1H, CH_2); 4.01 (d, 1H, J = 17.8 Hz, H-3a); 4.31 (d, 1H, H-3b); 7.70–7.74 (m, 2H, H-6′ and H-7′); 7.96 (d, 1H, J = 7.8 Hz, H-8′); 8.06 (d, 1H, J = 7.3 Hz, H-5′). FAB-MS *m*/*z* calcd for $C_{22}H_{23}N_3O_4S\cdot HCl$, 461.12; found, 461.31.

Data for 4-(2-Morpholino)ethyl-spiro[(dihydropirazin-2,5-dione)-6,3′-(2′,3′-dihydrothieno[2,3-*b*]naphtho-4′,9′-dione) Hydrochloride (6n). Yellow solid (46%), mp 185 °C (d). HPLC t_R 17.0 min. ^{1}H NMR (500 MHz, CD_3OD) δ 2.48–2.51 (m, 4H, CH_2); 2.75–2.78 (m, 2H, CH_2); 3.18 (d, 1H, J = 12.7 Hz, H-2′); 3.22–3.24 (m, 1H, CH_2); 3.41 (d, 1H, H-2″); 3.56–3.61 (m, 1H, CH_2); 3.63–3.71 (m, 4H, CH_2); 4.08 (d, 1H, J = 17.6 Hz, H-3a); 4.48 (d, 1H, H-3b); 7.74–7.79 (m, 2H, H-6′ and H-7′); 8.00 (d, 1H, J = 7.8 Hz, H-8′); 8.07 (d, 1H, J = 7.3 Hz, H-5′). MS [M^+] calcd for $C_{21}H_{21}N_3O_5S\cdot HCl$, 463.10; found, 463.32.

Data for 4-(2-Imidazo)ethylspiro[(dihydropirazin-2,5-dione)-6,3′-(2′,3′-dihydrothieno[2,3-*b*]naphtho-4′,9′-dione) Hydrochloride (6o). Yellow solid (48%), mp 182–184 °C. HPLC t_R 13.1 min. ^{1}H NMR (500 MHz, CD_3OD) δ 3.32 (d, 1H, J = 12.8 Hz, H-2′); 3.41–3.44 (m, 2H, CH_2 H-2″); 3.68–3.71 (m, 1H, CH_2); 3.96 (d, 1H, J = 17.6 Hz, H-3a); 3.95–3.98 (m, 1H, CH_2); 4.35 (d, 1H, H-3b); 6.98 (s, 1H, imidazol); 7.05 (s, 1H, imidazol); 7.60 (s, 1H, imidazol); 7.73–7.76 (m, 2H, H-6′ and H-7′); 7.92 (d, 1H, J = 7.8 Hz, H-8′); 8.00 (d, 1H, J = 7.3 Hz, H-5′). HPLC t_R 19.4 min. FAB-MS *m*/*z* calcd for $C_{20}H_{16}N_4O_4S\cdot HCl$, 444.07; found, 444.22.

Data for 4-(3-Imidazo)propylspiro[(dihydropirazin-2,5-dione)-6,3′-(2′,3′-dihydrothieno[2,3-*b*]naphtho-4′,9′-dione) Hydrochloride (6p). Yellow solid (50%), mp 182–184 °C. HPLC t_R 13.5 min. ^{1}H NMR (500 MHz, CD_3OD) δ 2.12–2.15 (m, 2H, CH_2); 3.01–3.04 (m, 1H, CH_2); 3.32 (d, 1H, J = 12.8 Hz, H-2′); 3.58 (d, 1H, H-2″); 3.86 (d, 1H, J = 17.7 Hz, H-3a); 3.92–3.94 (m, 1H, CH_2); 4.05–4.18 (m, 2H, CH_2); 4.24 (d, 1H, H-3b); 6.98 (s, 1H, imidazol); 7.05 (s, 1H, imidazol); 7.60 (s, 1H, imidazol); 7.73–7.76 (m, 2H, H-6′ and H-7′); 7.92 (d, 1H, J = 7.8 Hz, H-8′); 8.00 (d, 1H, J = 7.3 Hz, H-5′). ^{1}H NMR (500 MHz, D_2O) δ 2.10–2.13 (m, 3H, CH_2); 3.15–3.17 (m, 1H, CH_2); 3.66–3.69 (m, 2H, CH_2); 4.08 (dd, 2H, J = 12.8 Hz, H-2′); 4.21 (d, 1H, J = 17.7 Hz, H-3a); 4.31 (d, 1H, H-3b); 7.00 (s, 1H, imidazol); 7.09 (s, 1H, imidazol); 7.67 (s, 1H, imidazol); 7.79–7.82 (m, 2H, H-6′ and H-7′); 7.99 (d, 1H,

J = 6.8 Hz, H-8′); 8.02 (d, 1H, J = 7.0 Hz, H-5′). FAB-MS m/z calcd for $C_{21}H_{18}N_4O_4S \cdot HCl$, 458.08; found, 454.16.

Cell Lines. Human tumor cell lines were used in this study. MCF-7 breast carcinoma, SW 620 colon carcinoma, A549 lung carcinoma, HEK-293 kidney, M14 melanoma, and HeLa uterus cervical carcinoma, as well as one subline selected for resistance to doxorubicin (MCF-7/Dx). Sensitive tumor cells were obtained from American type Culture Collection, whereas resistant tumor cell were from Istituto Tumori of Milan. All cell lines were grown as monolayers in in RPMI-1640 (Life Technologies, Inc.) containing 10% fetal bovine serum (Life Technologies, Inc., NY).

Drug Treatment. For the cytotoxicity assay, cells were inoculated in a volume of 100 μL and at a density of 1500 per well in a 96-well microtiter plate. A 100 μL aliquot of complete medium was added to a cell-free well for a background subtraction. The seeded cells were preincubated for 24 h prior to addition of drugs in an atmosphere of 5% CO_2 and 95% air at 37 °C. Experimental agents **3** and **6a**−**6f** were solubilized in DMSO while **6g**−**6p** and doxorubicin were dissolved in water. Concentrated aliquots were stored frozen at −20 °C, thawed at room temperature immediately before use, diluted with complete medium, and added in a volume of 100 μL to the cell containing wells at twice the required final concentration. Each compound was initially tested at four 10-fold dilutions starting from 10^{-5} M. Following this prescreening, each compound was retested at various dilutions to more precisely determine the IC_{50}. The microtiter plates were then again placed in an incubator at 5% CO_2 and 95% air at 37 °C and incubated for an additional 24 h.

Sulforhodamine B Assay. At the end of the treatment, cell viability was assessed by the sulforhodamine B (SRB) assay.[23] Briefly, cells were fixed by adding 50 μL of ice-cold 50% (wt/vol) trichloroacetic acid (final concentration 10%) and incubating at 4 °C for 1 h. The supernatant was then discarded, and the microtiter plates were rinsed five times in deionized water. The plates were then dried overnight at room temperature in a fume hood. Next, 100 μL of a solution of SRB 0.4% (wt/vol) in 1% acetic acid was added to each well, and the plates were incubated for 30 min at room temperature. After removing unbound SRB by washing six times with 1% acetic acid, the plates were air-dried at room temperature. Finally, bound stain was solubilized with 10^{-2} M Tris buffer (pH = 10.5) and the optical density was read on an automatic spectrophotometer at a wavelength of 540 nm. The background optical density (complete medium plus stain, minus cells) was subtracted from the control well value, and the blank optical density (complete medium plus test compound plus stain, minus cells) was subtracted from the corresponding test well measurement. Data were expressed as $\%T/C$ = (OD of treated cells/OD of control cells) × 100, and the concentration of the test compound causing a 50% inhibition of cell growth (IC_{50}) was calculated from the dose/effect curve for each tested compound. Every assay was performed in triplicate, and the drug IC_{50} of each cell line was the average of at least three independent experiments.

Cell Proliferation Analysis. CaCo-2 cells (American type Culture Collection, Rockville, MD) were grown at 37 °C in h-glucose MEM containing 1% (by volume) MEM nonessential amino acids and supplemented with 10% (by volume) decomplemented FBS (Flow, McLean, VA), 100 U/mL penicillin, 100 μg/mL streptomycin, 1% L-glutamine, and 1% sodium pyruvate. The cells (17–21 passages) were grown in a humidified atmosphere of 95% air/5% CO_2 at 37 °C and were plated in six multiwell plates at different densities. After incubation for 4 h in DMEM with 10% FBS, the cells were washed with 1% PBS to remove unattached dead cells. Starved cells (DMEM without serum) were incubated with different times and concentrations of **6i** and **6l** derivatives and doxorubicin. All experiments were performed on triplicate cultures. For cell proliferation experiments on CaCo-2 cells, 1.0×10^5 cell/mL control and treated cells were seeded in 12 multiwell plates and incubated at 37 °C. After 12, 24, and 48 h, the cell number was determined with a hemocytometric counter and cell proliferation was determined through CyQuant cell proliferation assay Kit (Invitrogen, Milan) with dye fluorescence measurement at 480 nm excitation maximum and 520 nm emission maximum. Cell proliferation was expressed in percentage of proliferation compared with the control. All data are the mean ± SD of three experiments.

Flow Cytometry Analysis of Cell Cycle. CaCo-2 cells were seeded in six multiwell plates at the density of 25×10^5 cells/plate. After 48 h of incubation with **6i** and **6l** derivatives and doxorubicin in DMEM without serum at 37 °C, cells were washed in PBS, pelleted in centrifuged, and directly stained in a propidium iodide (PI) solution (50 mg PI in 0.1% sodium citrate, 0.1% NP40, pH 7.4) for 30 min at 4 °C in the dark. Flow cytometric analysis was performed using a FACScan flow cytometer (Becton Dickinson, San Jose, CA). To evaluate cell cycle PI fluorescence was collected as FL2 (linear scale) by the ModFIT software (Becton Dickinson). For the evaluation of intracellular DNA content, at least 20000 events for each point were analyzed in at least three different experiments giving a s.d. less than 5%.

Western Blot Assay. The effects of 3′*R*-**6k**, 3′*R*-**6l**, and doxorubicin on expression of Ciclyn A, were determined by Western blots. Compounds stimulated and unstimulated (control) cell lysates were prepared using an ice cold lysis buffer (50 mM Tris, 150 mM NaCl, 10 mM EDTA, 1% Triton) supplemented with a mixture of protease inhibitors containing antipain, bestatin, chymostatin, leupeptin, pepstatin, phosphoramidon, Pefabloc, EDTA, and aprotinin (Boehringer, Mannheim, Germany). Equivalent protein samples were resolved on 8–12% sodium dodecyl sulfate (SDS)−polyacrylamide gels and transferred to nitrocellulose membranes (Bio-Rad, Germany). For immunodetection, membranes were incubated overnight with specific antibodie at the concentrations indicated in manufacter's protocol (Santa Cruz Biotechnology). The antibody was diluted in Tris-buffered saline/Tween 20-1% milk powder. This step was followed by incubation with the corresponding horseradish peroxidase conjugated antibody (antirabbit-IgG 1:6000; Biosource, Germany). Bands were read by enhanced chemiluminescence (ECL-kit, Amersham, Germany).

STD-NMR Spectroscopy. STD-NMR experiments were performed on a Varian Inova 700 MHz spectrometer at 298 K. NMR samples were prepared by dissolving the ligand and the poly(dG-dC)·poly(dG-dC) copolymer (Pharmacia Biochemicals) in D_2O (600 μL, 99.996%, CIL Laboratories) containing phosphate-buffered saline at pH 7.1. A high ligand–receptor molar excess (20:1) was used for the best STD effects. In particular, the concentration of **6i** and **6p** was 1.0 mM, whereas that of the DNA was 50 μM, expressed as molarity of phosphate groups. The STD effects of the individual protons were calculated for each compound relative to a reference spectrum with off-resonance saturation at $\delta = -16$ ppm. Typically, 512 scans were recorded for each DF-STD spectrum (saturation time = 2 s). The relative STD effect was calculated for each signal as the difference between the intensity (expressed as S/N ratio) of one signal in the on-resonance STD spectrum and that of the same signal in the off-resonance NMR spectrum divided by the intensity of the same signal in the off-resonance spectrum. BMI values were obtained as ratio of the relative STD effects upon irradiation at 10.0 and −1.0 ppm.[22] A saturation power level (satpwr) of 10 dB was used. The absence of STD effects in samples in which the DNA was not added ensured a selective macromolecule saturation.

6i/DNA Complex Model. A model of **6i**/DNA interaction was obtained starting from the **3′**/DNA complex obtained in our previous work.[14] The model of compound **6i** was built using the Builder module of InsightII (Accelrys, San Diego, CA). It was energetically minimized using the steepest descent method for 10000 steps. The polycyclic portion of **6i** was then overlapped to the corresponding one of **3′** bound to the octamer $[d(ACGTACGT)]_2$.[14] The dimethyl(ethyl)amine side chain had a random conformation. Compound **3′** was removed, and the complex **6i**/DNA was extensively minimized using a combination of steepest descent and conjugate gradient algorithms until the maximum rms derivative was less than 0.01 kcal/Å. During the minimization, DNA atoms were tethered with a template force of 10 kcal/Å^2.

Acknowledgment. The FAB-MS and NMR spectral data were provided by Centro di Ricerca Interdipartimentale di Analisi Strumentale, Universita′ degli Studi di Napoli "Federico II". The assistance of the staff is gratefully appreciated.

Supporting Information Available: Microanalytical and ^{13}C NMR data for all test compounds. This material is available free of charge via the Internet at http://pubs.acs.org.

References

(1) De Vita, V. T.; Hellman, S.; Rosenberg, S. A. *Cancer: Principles and Practice of Oncology*, 6th ed.; Lippincott, Williams and Wilkins: Philadelphia, PA, 2001.

(2) Lown, J. W. Anthracycline and Anthraquinone Anticancer Agents: Current Status and Recent Developments. *Pharmacol. Ther.* **1993**, *60*, 185–214.

(3) Binaschi, M.; Bigioni, M.; Cipolline, A; Rossi, C.; Goso, C.; Maggi, C. A.; Capranico, G.; Animati, F. Anthracyclines: Selected New Developments. *Curr. Med. Chem. Anti-Cancer Agents* **2001**, *1*, 113–130.

(4) Thigpen, J. T. Innovations in Anthracycline Therapy: Overview. *Community Oncol.* **2005**, *2* (S1), 3–7.

(5) Cheng, C. C.; Zee-Cheng, R. K. Y. The Design, Synthesis and Development of a New Class of Potent Antineoplastic Anthraquinones. *Prog. Med. Chem.* **1983**, *20*, 83–118.

(6) Gerwirtz, D. A. A Critical Evaluation of the Mechanisms of Action Proposed for the Antitumor Effects of the Antrhracycline Antibiotics Adriamycin and Daunorubicin. *Biochem. Pharmacol.* **1999**, *57*, 727–741.

(7) Krishna, R.; Mayer, L. D. Multidrug Resistance (MDR) in Cancer. Mechanisms, Reversal Using Modulators of MDR and the Role of MDR Modulators in Influencing the Pharmacokinetics of Anticancer Drugs. *Eur. J. Pharm. Sci.* **2000**, *11*, 265–83.

(8) Baird, R. D.; Kaye, S. B. Drug Resistance Reversal—Are We Getting Closer. *Eur. J. Cancer* **2003**, *39*, 2450–2461.

(9) Minotti, G.; Menna, P.; Salvatorelli, E.; Cairo, G.; Gianni, L. Anthracyclines: Molecular Advances and Pharmacologic Developments in Antitumor Activity and Cardiotoxicity. *Pharmacol. Rev.* **2004**, *56*, 185–229.

(10) Serrano, J.; Palmeira, C. M.; Kuehl, D. W.; Wallace, K. B. Cardioselective and Cumulative Oxidation of Mitochondrial DNA Following Subchronic Doxorubicin Administration. *Biochim. Biophys. Acta* **1999**, *1411*, 201–205.

(11) Gomez-Monterrey, I.; Campiglia, P; Mazzoni, O.; Novellino, E.; Diurno, M. V. Cycloaddition Reactions of Thiazolidine Derivatives. An Approach to the Synthesis of New Functionalized Heterocyclic Systems. *Tetrahedron Lett.* **2001**, *42*, 5755–5757.

(12) Gomez-Monterrey, I.; Campiglia, P.; Grieco, P.; Diurno, M. V.; Bolognese, A.; La Colla, P.; Novellino, E. New Benzo[*g*]isoquinoline-5,10-diones and Dihydrothieno[2,3-*b*]naphtho-4,9-dione Derivatives: Synthesis and Biological Evaluation as Potential Antitumoral Agents. *Bioorg. Med. Chem.* **2003**, *11*, 3769–3775.

(13) Gomez-Monterrey, I.; Santelli, G.; Campiglia, P.; Califano, D.; Falasconi, F.; Pisano, C.; Vesci, L.; Lama, T.; Grieco, P.; Novellino, E. Cytotoxic Evaluation of Novel Spirohydantoin Derivatives of the Dihydrothieno[2,3-*b*]naphtho-4,9-dione System. *J. Med. Chem.* **2005**, *48*, 1152–1157.

(14) Gomez-Monterrey, I.; Campiglia, P.; Carotenuto, A.; Califano, D.; Pisano, C.; Vesci, L.; Lama, T.; Bertamino, A.; Sala, M.; Mazzella di Bosco, A.; Grieco, P.; Novellino, E. Design, Synthesis, and Cytotoxic Evaluation of a New Series of 3-Substituted Spiro[(dihydropyrazine-2,5-dione)-6,3′-(2′,3′-dihydrothieno[2,3-*b*]naphtho-4′,9′-dione)] Derivatives. *J. Med. Chem.* **2007**, *50*, 1787–1798.

(15) Martínez, R.; Chacón-García, L. The Search of DNA-Intercalators as Antitumoral Drugs: What it Worked and What did not Work. *Curr. Med. Chem.* **2005**, *12*, 127–151.

(16) Rittle, K. E.; Evans, B. E.; Bock, M. G.; Di Pardo, R. M.; Whitter, W. L.; Homnick, C. F.; Veber, D. F.; Freidinger, R. M. A New Amine Resolution Method and Its Application to 3-Amino Benzodiazepines. *Tetrahedron Lett.* **1987**, *28*, 521–522.

(17) Hande, K. R. Topoisomerase II inhibitors. *Update Cancer Ther.* **2006**, *1*, 3–15.

(18) (a) Pinto, M.; Robine-Leon, S.; Appay, M. D.; Kedinger, M.; Triadou, N.; Dussaulx, E.; Lacroix, B.; Simon-Assman, P.; Haffen, K.; Fogh, J.; Zweibaum, A. Enterocyte-like Differentiation and Polarization of the Human Colon Carcinoma Cell Line CaCo-2 in Culture. *Biol. Cell* **1983**, *47*, 323–330. (b) Engle, M. J.; Goetz, G. S.; Alpers, D. H. CaCo-2 Cells Express a Combination of Colonocyte and Enterocyte Phenotypes. *J. Cell. Physiol.* **1998**, *174*, 362–369.

(19) Yam, C. H.; Fung, T. K.; Poon, R. Y. C. Cyclin A in Cell Cycle Control and Cancer. *Cell. Mol. Life Sci.* **2004**, *59*, 1317–1326.

(20) Mayer, M.; Meyer, B. Characterization of Ligand Binding by Saturation Transfer Difference NMR Spectroscopy. *Angew. Chem., Int. Ed.* **1999**, *38*, 1784–1788.

(21) Meyer, B.; Peters, T. NMR Spectroscopy Techniques for Screening and Identifying Ligand Binding to Protein Receptors. *Angew. Chem., Int. Ed.* **2003**, *42*, 864–890.

(22) Di Micco, S.; Bassarello, C.; Bifulco, G.; Riccio, R.; Gomez-Paloma, L. Differential-Frequency Saturation Transfer Difference NMR Spectroscopy Allows the Detection of Different Ligand—DNA Binding Modes. *Angew. Chem., Int. Ed.* **2006**, *45*, 224–228.

(23) Skehan, P.; Storeng, R.; Scudiero, D.; Monks, A.; McMahon, J.; Vistica, D.; Warren, J. T.; Bokesch, H.; Kenney, S.; Boyd, M. R. New Colorimetric Cytotoxicity Assay for Anticancer-Drug Screening. *J. Natl. Cancer Inst.* **1990**, *82*, 1107–1112.

JM7013056